Numerical Implementation of Wavelength-Dependent Photonic Spike Timing Dependent Plasticity Based on VCSOA

Shuiying Xiang, Junkai Gong, Yahui Zhang, Xingxing Guo, Yanan Han, Aijun Wen, and Yue Hao

***Abstract*— We propose to realize photonic spike timing dependent plasticity (STDP) by using a vertical-cavity semiconductor optical amplifier (VCSOA) subject to dual optical pulse injections. The computational model of the photonic STDP is presented for the first time based on the well-known Fabry–Pérot approach. Through numerical simulations, the dependences of photonic STDP on the bias current of VCSOA and the input powers are analyzed carefully. Besides, the effect of the initial wavelength detuning on the photonic STDP is also explored. It is found that, the current scheme requires much lower bias current and input power to obtain controllable STDP curve when compared with the previously reported photonic STDP circuits; the initial wavelength detuning is an effectively controllable parameter to realize wavelength-dependent photonic STDP. The computational model of the photonic STDP based on a VCSOA is interesting and valuable for numerically simulating of large-scale photonic spiking neural network, and provides a guideline to design low power consumption photonic neuromorphic systems.**

***Index Terms*— Vertical-cavity semiconductor optical amplifier, photonic spike timing dependent plasticity, photonic neuromorphic systems, dual optical pulse injections, lower power consumption.**

I. Introduction

THE photonic neuromorphic computing, which inherits the advantages of both photonics and brain-like computing, revolutionizes the computation paradigm compared to the conventional von Neumann approach, and has attracted extensive interest in recent years [1]. It has been demonstrated that, the precise spike timing carries important information [2]–[4], and the spike timing dependent plasticity (STDP) is closely related to the learning and memory in the brain [5], [6]. In the context of photonic spike processing, the photonic spiking neuron and photonic synapse are two basic functional elements of photonic spiking neural network (SNN). When designing the photonic neuromorphic devices, low power consumption is one of the key requirements.

Recently, many photonic devices have been proposed to experimentally and numerically emulate the spiking dynamics [7]–[16], as well as the STDP [17]–[21]. For example, the first photonic STDP circuit was demonstrated by Fok *et al*. [17] in an experiment in which a semiconductor optical amplifier (SOA) and an electro-absorption modulator (EAM) were utilized. The STDP curve with variable potentiation and depression windows could be achieved by varying the EAM bias and SOA current. The proposed photonic STDP operated on picosecond time scale, and was much faster than the biological counterpart. Besides, a photonic STDP using a single SOA was also experimentally realized [18]. Moreover, the supervised and unsupervised learning algorithms based on the photonic STDP were further explored [20]. Ren *et al*. experimentally implemented a photonic STDP with a feedback signal; they proposed to introduce a modulatory signal into the original photonic STDP scheme by varying the current of two SOAs. The reward-based reinforcement learning was also realized based on the proposed photonic STDP [19].

However, in these reported photonic STDP circuits based on the conventional in-plane traveling-wave SOA, the operating current of SOA is usually large, i.e., several tens of or hundreds of mA. This is undesirable for low power consumption neuromorphic computing applications. In addition, the large-scale integration of photonic SNN is limited by the photonic synapse based on in-plane SOA. Furthermore, a computational model of photonic STDP has not yet been reported, which is highly desirable for the numerical simulation of large-scale photonic SNN.

Note that, various emerging optical devices which could be highly integratable have been reported [22]–[29], and are believed to be interesting for on-chip photonic neuromorphic systems. Among these, vertical-cavity

Manuscript received July 30, 2018; revised October 25, 2018; accepted October 30, 2018. Date of publication November 5, 2018; date of current version November 19, 2018. This work was supported in part by the National Natural Science Foundation of China under Grant 61674119, in part by the Postdoctoral Innovation Talent Program in China under Grant BX201600118, in part by the Young Talent fund of University Association for Science and Technology in Shaanxi, China, under Grant 20160109, in part by the Project Funded by China Postdoctoral Science Foundation under Grant 2017M613072, in part by the Natural Science Basic Research Plan in Shaanxi Province of China under Grant 2017JM6002 and Grant 2016JM6009, and in part by the China 111 Project under Grant B08038. *(Corresponding author: Shuiying Xiang.)*

S. Xiang is with the State Key Laboratory of Integrated Service Networks, Xidian University, Xi'an 710071, China, and also with the State Key Discipline Laboratory of Wide Bandgap Semiconductor Technology, School of Microelectronics, Xidian University, Xi'an 710071, China (e-mail: jxxsy@126.com).

J. Gong, Y. Zhang, X. Guo, Y. Han, and A. Wen are with the State Key Laboratory of Integrated Service Networks, Xidian University, Xi'an 710071, China.

Y. Hao is with the State Key Discipline Laboratory of Wide Bandgap Semiconductor Technology, School of Microelectronics, Xidian University, Xi'an 710071, China.

Color versions of one or more of the figures in this paper are available online at http://ieeexplore.ieee.org.

Digital Object Identifier 10.1109/JQE.2018.2879484

devices become energy-efficient solutions in many applications including optical signal processing and optical interconnecting [7], [8], [13]–[16], [24], [28]. As a typical vertical-cavity device, the vertical-cavity surface-emitting laser (VCSEL) has attracted lots of attention in the photonic neuron due to its low power consumption and rich polarization dynamics [7], [8], [10], [13]–[16]. Actually, when operating below threshold, the VCSEL can serve as a Fabry–Pérot (FP) amplifier, also referred to as a vertical-cavity semiconductor optical amplifier (VCSOA) [30], [31]. For instance, A. Hurtado et al employed a commercial 1550 nm VCSEL fabricated by Vertilas as the VCSOA, and experimentally observed power and wavelength bistability and nonlinear gain [30]. Compared to the conventional in-plane SOA, VCSOA exhibits many appealing advantages such as low cost, polarization insensitivity, high fiber coupling efficiency, on wafer testing, and ease of fabricating two-dimensional arrays [30]–[32]. However, the photonic synapse based on the VCSOA has not yet been reported.

In this paper, we propose to implement photonic STDP by using a VCSOA and aim to present a computational model for the photonic STDP with low power consumption. The wavelength-dependent photonic STDP is numerically achieved for the first time, to the best of our knowledge. Note that, in our previous works, we have numerically emulated the spike dynamics of VCSELs with the advantages of ease of integration and low power consumption [10], [13], [15], [16]. Hence, by properly setting the bias current of the VCSEL, a large-scale photonic SNN consisting of VCSELs, acting as both photonic neurons and synapses, can be expected. The rest of this paper is organized as follows. In Section II, the theoretical model of a VCSOA is presented. In Section III, the photonic STDP properties are carefully considered through extensive numerical simulation. The effects of the bias current, input powers, and the initial wavelength detuning are examined. Finally, conclusions are drawn in Section IV.

II. Theory and Model

The schematic diagram of the photonic STDP based on the VCSOA subject to two optical pulse injections is illustrated in Fig. 1. In this scheme, Pulse 1 and Pulse 2 are two optical pulse injection beams, corresponding to pre-synaptic and post-synaptic spikes, respectively. The relative time delay between two injection beams can be controlled precisely by a variable optical delay line (VODL). For simplicity, we consider the injection beam without (with) the VODL as the control beam (signal beam). Note, in Fig. 1, we present two injection cases. For case A, the presynaptic spike (Pulse 1) is considered as a control beam with fixed arrival time, whereas the post-synaptic spike (Pulse 2) is considered as a signal beam with variable arrival time. For case B, the two optical injection beams are exchanged, i.e., the post-synaptic spike (Pulse 2) becomes the control beam, the pre-synaptic spike (Pulse 1) is connected with the VODL and becomes the signal beam. For convenience, we denote $P_{c,s}(\lambda_{c,s})$ as the input power (wavelength) of control and signal beams, which have been clearly defined in Fig. 1. A three-port optical circulator is

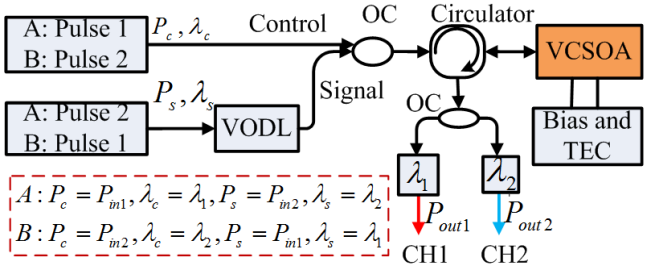

Fig. 1. Schematic diagram of the proposed photonic STDP based on VCSOA. Pulse 1 (Pulse 2): the optical pulse injection beam corresponding to pre-synaptic (post-synaptic) spike; $P_{c,s}(\lambda_{c,s})$ denotes the input power (wavelength) of control and signal beams; $P_{in1,in2}$ ($\lambda_{1,2}$) denotes the input power (wavelength) of two injection pulses; VODL: variable optical delay line, OC: optical coupler; Circulator: optical circulator; VCSOA: vertical-cavity semiconductor optical amplifier; Bias and TEC: the bias current and temperature controller for the VCSOA; $\lambda_{1,2}$ in the box means a bandpass filter; CH1 (CH2): output channel.

used to inject the two optical pulse beams into the VCSOA. The reflective outputs of the VCSOA are then filtered to separate the two beams with different wavelengths. The outputs at different relative time delays for both cases are then utilized to study the property of the photonic STDP based on a VCSOA.

The most popular methods to numerically study the FP SOAs are the rate equation approach and the FP approach [33]–[38]. The FP approach was initially derived by Adams [39] and has been successfully applied to investigate the characteristics of the VCSOA [32], [38]. Besides, the FP approach includes only one rate equation for the carrier density, and thus is computationally efficient, which is highly desirable for numerical simulation of large-scale photonic SNN.

We extend the FP approach and numerically study the photonic STDP based on a VCSOA subject to dual optical pulse injection beams. The rate equation for the carrier density N can be written as follows [32], [39]:

$$\frac{dN}{dt} = \frac{\eta I}{e\Gamma_1 V} - (AN + BN^2 + CN^3) - \frac{\Gamma c\xi a(N - N_0)}{n_c}(\beta_{sp} S_{ase} + S_1 + S_2) \quad (1)$$

where I is the bias current of VCSOA. S_{ase} denotes the averaged spontaneous photon density, S_1 and S_2 represent the averaged stimulated photonic density related to the dual optical pulse injection beams. These averaged photonic density terms can be expressed as [32] and [39]:

$$S_{ase} = \left(\frac{(G_s - 1)[(1 - R_b)(1 + R_t G_s) + (1 - R_t)(1 + R_b G_s)]}{gL_c(1 - R_t R_b e^{2gL_c})} - 2\right) \times \frac{\Gamma_1 B N^2 n_c}{gc} \quad (2)$$

$$S_{1,2} = \left(\frac{(1 - R_t)(1 + R_b G_s)(G_s - 1)}{(1 - \sqrt{R_t R_b} G_s)^2 + 4\sqrt{R_t R_b} G_s \sin^2 \Phi_{1,2}}\right) \frac{P_{in1,in2} n_c \lambda_p}{hc^2 V g} \quad (3)$$

TABLE I
SOME TYPICAL PARAMETERS OF VCSOA USED IN SIMULATION [32]

Param.	Description	Value
R_t	Top DBR reflectivity	0.9961
R_b	Bottom DBR reflectivity	0.9975
n_c	Cavity refractive index	3.2
V	Cavity volume	$5.71\times10^{-18}\,\mathrm{m}^3$
L_c	Effective cavity length	$1.25\lambda_p n_c$
b	Linewidth enhancement factor	2.15
a	Linear material gain coefficient	$2.1\times10^{-20}\,\mathrm{m}^2$
α_i	Average cavity loss coefficient	$1360\mathrm{m}^{-1}$
ξ	Gain enhancement factor	1.9982
η	Internal quantum efficiency	0.4
Γ	Lateral confinement factor	1
Γ_1	Longitudinal confinement factor	0.02146
A	Nonradiative recombination rate	$1\times10^{8}s^{-1}$
B	Radiative recombination coefficient	$1\times10^{-16}\,\mathrm{m}^6s^{-1}$
C	Auger recombination coefficient	$5\times10^{-42}\,\mathrm{m}^6s^{-1}$
N_0	Transparency carrier density	$2\times10^{24}\,\mathrm{m}^{-3}$
β_{sp}	Spontaneous emission factor	2×10^{-5}

where $G_s = e^{gL_c}$ denotes the single-pass gain, and $g = \Gamma\Gamma_1\xi a(N-N_0)-\alpha_i$. The single-pass phase change considering the dependence of the index of refraction on the carrier density can be described as [32], [36], and [37]:

$$\Phi_{1,2} = \Phi_{01,02} - b\Gamma\Gamma_1\xi L_c a(N-N_s)/2 \tag{4}$$

where the second term couples the optical phase to the carrier density in the amplifier. N_s denotes the carrier density when the optical pulse beams are not injected into the VCSOA. The terms $\Phi_{01,02} = 2\pi n_c L_c(1/\lambda_{1,2} - 1/\lambda_p)$ represent the initial phase detuning, $\lambda_p = 1550.3$nm is the peak resonant wavelength of the VCSOA, and $\lambda_{1,2}$ denote wavelengths of optical pulse injection beams. We further introduce the initial wavelength detuning as $\Delta\lambda_1 = \lambda_1 - \lambda_p$, $\Delta\lambda_2 = \lambda_2 - \lambda_p$. $P_{in1,in2}$ account for the optical power of two optical pulse injection beams, respectively. In our work, we simply consider Gaussian pulse as the input. The relative time delay difference between two injection beams is defined as $\Delta t = t_2 - t_1$, where t_1 and t_2 denote the peak location of two optical pulses. The parameters e, h, c denote the electron charge, the Planck constant, the speed of light, respectively. The other parameters are defined in Table 1. We numerically solve the equations using the fourth-order Runge-Kutta method.

The amplifier gain for a VCSOA operating in reflection mode can be described as [32] and [39]:

$$G_{\mathrm{R1,R2}} = \frac{(\sqrt{R_t}-\sqrt{R_b}G_s)^2 + 4\sqrt{R_tR_b}G_s\sin^2\Phi_{1,2}}{(1-\sqrt{R_tR_b}G_s)^2 + 4\sqrt{R_tR_b}G_s\sin^2\Phi_{1,2}} \tag{5}$$

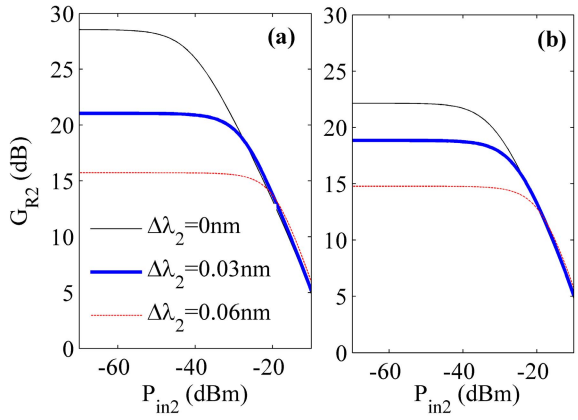

Fig. 2. The values of G_{R2} as functions of input power for different cases of initial wavelength detuning, (a) $I = 0.64$mA, (b) $I = 0.6$mA, with $P_{in1} = 0$.

Then the output power can be calculated by $P_{out1,out2} = P_{in1,in2}G_{R1,R2}$.

III. NUMERICAL RESULTS

In this section, we first consider the gain and carrier density dynamics, and then examine carefully the effects of the input powers and bias current on the STDP property. As a significant difference between the VCSOA and the in-plane traveling-wave SOA, the effect of initial wavelength detuning is still needed to be explored due to the existence of the peak resonant wavelength of VCSOA.

At first, we consider the case in which the VCSOA is subjected to only single optical pulse injection in order to analyze the gain property. Here, we assume $P_{in1} = 0$. The values of G_{R2} as functions of input power for different cases of bias current and initial wavelength detuning are presented in Fig. 2. It can be observed that, the small-signal gain is lower for a larger $\Delta\lambda_2$, but the large-signal gain after saturation for a given P_{in2} is almost the same for different $\Delta\lambda_2$. Besides, a lower bias current leads to smaller G_{R2} for a given $\Delta\lambda_2$.

Next, we consider that two optical pulses are injected into the VCSOA at different times. The temporal evolutions of carrier density for different cases of P_{in1} are presented in Fig. 3 for $\Delta t = 500$ps. It can be seen that, when the first pulse arrives at $t_1 = 20$ns, the value of N decreases sharply due to the stimulated recombination, and then recovers slowly. The second pulse is amplified with reduced gain due to the carrier depletion, when it arrives before the carrier density is totally recovered, [19], [21]. Besides, one can find that, a larger P_{in1} leads to a smaller N at $t_1 = 20$ns. Therefore, a larger recovery time is required.

By fixing the arrival time of the control beam, and varying the arrival time of the signal beam, one can obtain the STDP curve according to the recording data at two output channels [21]. The mechanism for the photonic STDP is presented in Fig. 4. As both injection cases A and B shown in Fig. 1 should be included to obtain the STDP curves, we also define $\Delta\lambda_c = \lambda_c - \lambda_p$, $\Delta\lambda_s = \lambda_s - \lambda_p$ for convenience. In both injection cases, we assume that $P_c = 25\mu w$, $P_s = 5\mu w$, $\Delta\lambda_c = 0$nm and $\Delta\lambda_s = 0.06$nm. As shown in Fig. 4 (a), for case A, the control pulse (Pulse 1) enters the VCSOA at

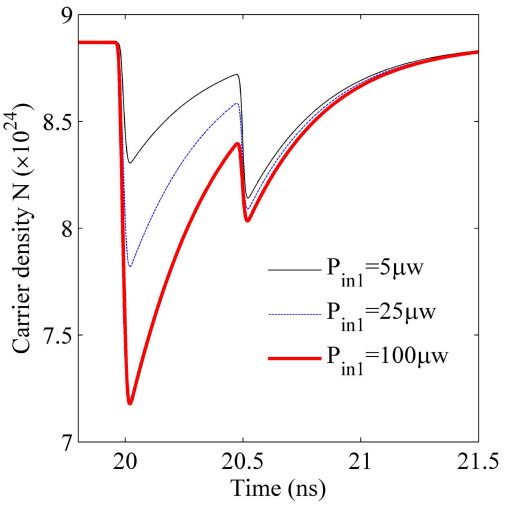

Fig. 3. The carrier density dynamics for VCSOA under dual optical pulse injection beams for different cases of P_{in1}, with $\Delta t = 500$ps, $I = 0.6$mA, $P_{in2} = 5\mu w$.

$t_1 = 20$ns, while the arrival time of Pulse 2 is varied according to Δt. When the signal beam (Pulse 2) enters the VCSOA first, i.e., $t_2 < t_1 = 20$ns or $\Delta t < 0$, the peak values of P_{out2} for each Δt are almost constant as the signal beam is amplified without the influence of VCSOA's carrier depletion. The constant peak power is denoted as $P_{2\max}$. On the other hand, when the control beam enters the VCSOA first, i.e., $t_2 > t_1 = 20$ns or $\Delta t > 0$, the signal beam, arriving within the recovery time, experiences carrier depletion induced by the preceding control beam. The peak power for a given Δt is denoted as $\max[P_{out2}(t)]$. As can be seen from the right side of Fig. 4(b), $\max[P_{out2}(t)]$ is smaller than $P_{2\max}$ and is increased with Δt due to the carrier recovery. The loss of output power at a given Δt $\Delta P_2(\Delta t) = P_{2\max} - \max[P_{out2}(t)]$, corresponds to the magnitude of weight update of the STDP potentiation window [19]. Correspondingly, for injection case B, the inputs and outputs are presented in Figs.4(c) and (d). It can be seen that, when $\Delta t > 0$, i.e., $t_1 < t_2 = 20$ns, the peak values of P_{out1} for each case of Δt are almost constant, and are denoted as $P_{1\max}$. When $\Delta t < 0$, i.e., $t_1 > t_2$, the lagging signal beam (Pulse 1) that arrives within the recovery time experiences carrier depletion induced by the control beam (Pulse 2). The peak power for a given Δt is denoted as $\max[P_{out1}(t)]$. Similarly, $\Delta P_1(\Delta t) = \max[P_{out1}(t)] - P_{1\max}$, corresponds to the magnitude of weight update of the STDP depression window [19].

Hence, after recoding all the outputs at each Δt as shown in Figs.4 (b) and (d) for both cases A and B, the $\Delta\omega_{1,2}(\Delta t)$ can be calculated from each output channel by [19] and [21]:

$$\Delta\omega_{1,2}(\Delta t) = \begin{cases} (P_{1,2\max} - \max[P_{out1,2}(t)])/P_{1,2\max}, & if\ \ \Delta t > 0 \\ (\max[P_{out1,2}(t)] - P_{1,2\max})/P_{1,2\max}, & else \end{cases} \quad (6)$$

Then, the STDP curve can be obtained by:

$$\Delta\omega(\Delta t) = \begin{cases} \Delta\omega_2(\Delta t), & if\ \ \Delta t > 0 \\ \Delta\omega_1(\Delta t), & if\ \ \Delta t < 0 \end{cases} \quad (7)$$

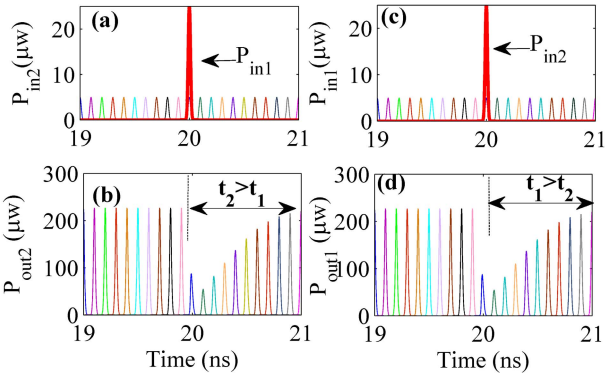

Fig. 4. (a,c) The input pulses, (b,d) output pulses, with $I = 0.6$mA, the power of control (signal) beam is $P_c = 25\mu w (P_s = 5\mu w)$, the initial wavelength detuning values are $\Delta\lambda_c = 0$nm and $\Delta\lambda_s = 0.06$nm for both injection cases.

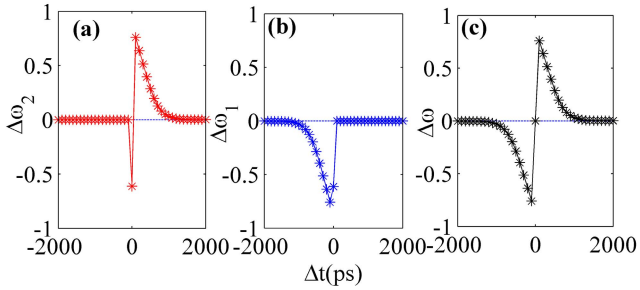

Fig. 5. (a) The calculated $\Delta\omega_2$ corresponding to Fig. 4(b), (b) $\Delta\omega_1$ corresponding to Fig. 4(d), (c) the STDP curve.

From a practical viewpoint, e.g., unsupervised learning based on STDP, if the pre-synaptic and post-synaptic neurons fire spikes simultaneously, the update of synaptic weight is no longer needed. Hence, for $\Delta t = 0$, we simply denote $\Delta\omega(0) = 0$.

The calculated $\Delta\omega_{1,2}$ as well as the final STDP curve are presented in Fig. 5. Here, $\Delta\omega_2$ is calculated based on the recording outputs in Fig. 4(b), and $\Delta\omega_1$ is calculated based on the outputs in Fig. 4(d). By combing the right half side of Fig. 5(a) and the left half side of Fig. 5(b), the STDP curve is obtained. Note that, the STDP curve shown in Fig. 5(c) is similar to the biological experiment, but at a much faster time scale [5], [6]. The width of the potentiation or depression window of the proposed photonic STDP based on VCSOA is extended to more than 800ps, which is close to the experimentally measured gain recovery time [38]. In addition, compared with the previously reported photonic STDP based on a conventional in-plane SOA, the STDP window based on a VCSOA is much wider, and the required bias current and input powers are much lower. Note that, such low power consumption property is highly desirable for photonic neuromorphic systems.

The STDP curves for different bias currents under two cases of initial wavelength detuning are presented in Fig. 6. It can be observed that, for $\Delta\lambda_s = -0.03$nm, a larger I leads to larger height and smaller width of STDP window, which is similar to the experimental findings obtained for in-plane SOAs [19], [21]. However, for $\Delta\lambda_s = 0.06$nm,

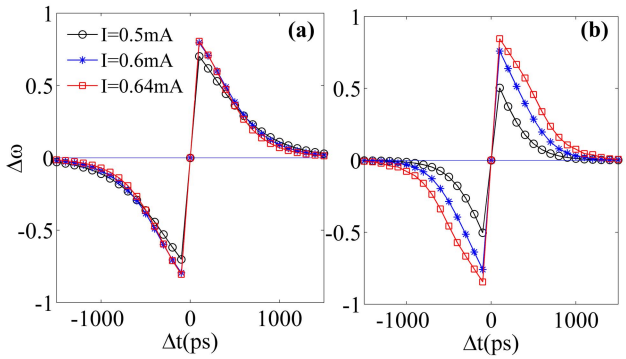

Fig. 6. Photonic STDP curves for different bias currents. (a) $\Delta\lambda_s = -0.03$nm, (b) $\Delta\lambda_s = 0.06$nm, with $P_c = 25\mu w$, $P_s = 5\mu w$, $\Delta\lambda_c = 0$.

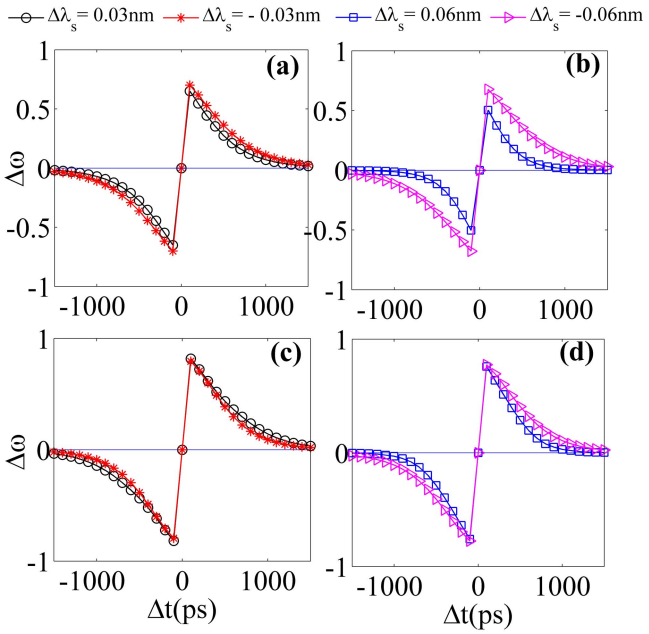

Fig. 7. Photonic STDP curves for different initial wavelength detuning, (a, b) $I = 0.5$mA, (c, d) $I = 0.6$mA, with $P_c = 25\mu w$, $P_s = 5\mu w$, $\Delta\lambda_c = 0$.

as I is increased, the height of STDP window is increased, and this is also the case for the width of STDP window. That is to say, because of the resonant peak of the VCSOA, the STDP curve can also be slightly controlled by the initial wavelength detuning, which has not been previously reported in the photonic STDP to the best of our knowledge.

For comparison purpose, the photonic STDP curves for different cases of initial wavelength detuning under two bias current conditions are further presented in Fig. 7. The results show that, for $\Delta\lambda_s = \pm 0.03$nm, the width of STDP window for the negative case is slightly larger than the positive case when $I = 0.5$mA. However, for $I = 0.6$mA, the opposite trend is observed. For $\Delta\lambda_s = \pm 0.06$nm, the width of STDP window for the negative case is slightly larger than the positive case for both $I = 0.5$mA and $I = 0.6$mA. Hence, the combined effects of initial wavelength detuning and bias current on the STDP curves are interesting, which may be attributed to the wavelength-dependent gain property of VCSOA [37], [38],

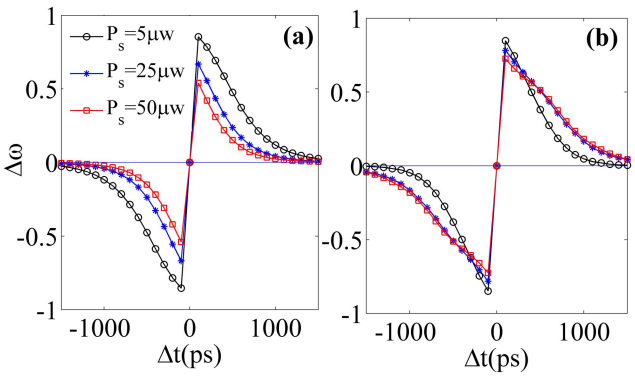

Fig. 8. Photonic STDP curves for different P_s. (a) $\Delta\lambda_s = -0.03$nm, (b) $\Delta\lambda_s = 0.06$nm, with $I = 0.6$mA, $P_c = 50\mu w$, $\Delta\lambda_c = 0$.

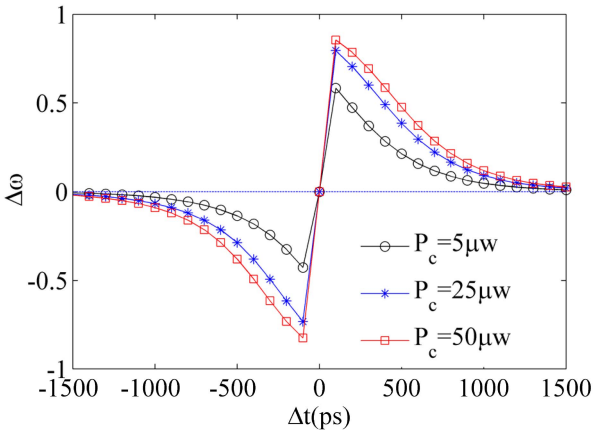

Fig. 9. Photonic STDP curves for different P_c,with $I = 0.6$mA, $P_s = 5\mu$w, $\Delta\lambda_s = 0.06$nm, $\Delta\lambda_c = 0$.

and may motivate further experimental demonstration of such wavelength- dependent photonic STDP based on the VCSOA.

Next, we present the STDP curves for different input powers of the signal beam in Fig. 8. It can be seen that, on the one hand, for $\Delta\lambda_s = -0.03$nm, a larger (smaller) P_s leads to decreased (increased) height and decreased (increased) width of the STDP curves. On the other hand, for $\Delta\lambda_s = 0.06$nm, a larger (smaller)P_s leads to decreased (increased) height and increased (decreased) width of the STDP curves. Hence, tunable STDP curves can be achieved by simply adjusting the input power of the signal pulse.

Correspondingly, the STDP curves for different input powers of the control beam are presented in Fig. 9. It is shown that, a higher (lower) input power leads to the increase (decrease) of both width and height of STDP window. Here, the preceding control beam with higher input power consumes more carriers due to the stimulated emission. When the Δt is relatively small, the partially recovered carriers in VCSOA give rise to less gain. Therefore, the height of STDP window becomes larger. In addition, for a larger P_c, a larger recovery time is required to approach the carrier density at the stable state with the effort of the continuous current injection, which corresponds to larger width of STDP window. We have performed similar calculations for $\Delta\lambda_s = -0.03$nm, and obtain similar

trends (not shown here), which may be associated with the fact that the wavelength of the control pulse is set to be equal to the peak resonant wavelength of VCSOA.

Hence, by the numerical calculation based on the FP approach of a VCSOA, we find that the wavelength-dependent photonic STDP can be achieved. Tunable STDP curves can be obtained by simply adjusting the bias current of the VCSOA, the input power of the control pulse or signal pulse, as well as the initial wavelength detuning.

IV. Conclusion

In summary, we have proposed photonic implementation of STDP based on the VCSOA, and presented a computational model of the photonic STDP for the first time, to our knowledge. Compared to the photonic STDP based on in-plane SOAs, much lower bias current and input power are required in our proposed scheme based on the VCSOA. Besides, minor control of the photonic STDP curve can be obtained by properly adjusting the bias current of the VCSOA as well as the input power. In particular, as a consequence of the peak resonant wavelength of the VCSOA, the wavelength-dependent STDP can be achieved, which is quite different from the previously reported result. This work provides a computational model of the photonic STDP based on a VCSOA, which is valuable for numerical simulation of large-scale photonic SNN, and helpful for paving the way for low power consumption photonic neuromorphic computing.

Acknowledgment

The authors would like to thank Prof. Michael Adams at University of Essex, and Dr. Antonio Hurtado at University of Strathclyde, and Dr. Jianji Dong at Huazhong University of Science & Technology for their helps and discussions. S. Xiang would like to thank Dr. Nianqiang Li at the University of Ottawa for careful proofreading.

References

[1] P. R. Prucnal, B. J. Shastri, T. F. de Lima, M. A. Nahmias, and A. N. Tait, "Recent progress in semiconductor excitable lasers for photonic spike processing," *Adv. Opt. Photon.*, vol. 8, no. 2, pp. 228–299, May 2016.

[2] T. Gollisch and M. Meister, "Rapid neural coding in the retina with relative spike latencies," *Science*, vol. 319, no. 5866, pp. 1108–1111, Feb. 2008.

[3] J. J. Hopfield, "Pattern recognition computation using action potential timing for stimulus representation," *Nature*, vol. 376, no. 6535, pp. 33–36, 1995.

[4] Z. F. Mainen and T. J. Sejnowski, "Reliability of spike timing in neocortical neurons," *Science*, vol. 268, no. 5216, pp. 1503–1506, 1995.

[5] G. Q. Bi and M. M. Poo, "Synaptic modifications in cultured hippocampal neurons: Dependence on spike timing, synaptic strength, and postsynaptic cell type," *J. Neurosci.*, vol. 18, no. 24, pp. 10464–10472, 1998.

[6] G.-Q. Bi and M.-M. Poo, "Synaptic modification by correlated activity: Hebb's postulate revisited," *Annu. Rev. Neurosci.*, vol. 24, pp. 139–166, Mar. 2001.

[7] A. Hurtado, K. Schires, I. D. Henning, and M. J. Adams, "Investigation of vertical cavity surface emitting laser dynamics for neuromorphic photonic systems," *Appl. Phys. Lett.*, vol. 100, no. 10, p. 103703, Mar. 2012.

[8] M. A. Nahmias, B. J. Shastri, A. N. Tait, and P. R. Prucnal, "A leaky integrate-and-fire laser neuron for ultrafast cognitive computing," *IEEE J. Sel. Top. Quantum Electron.*, vol. 19, no. 5, Sep./Oct. 2013, Art. no. 1800212.

[9] B. J. Shastri, M. A. Nahmias, A. N. Tait, A. W. Rodriguez, B. Wu, and P. R. Prucnal, "Spike processing with a graphene excitable laser," *Sci. Rep.*, vol. 6, p. 19126, Jan. 2016.

[10] S. Xiang, A. Wen, and W. Pan, "Emulation of spiking response and spiking frequency property in VCSEL-based photonic neuron," *IEEE Photon. J.*, vol. 8, no. 5, Sep. 2016, Art. no. 1504109.

[11] R. Wang, C. Qian, Q. Ren, and J. Zhao, "Optoelectronic neuromorphic system using the neural engineering framework," *Appl. Opt.*, vol. 56, no. 5, pp. 1517–1525, Feb. 2017.

[12] A. N. Tait *et al.*, "Neuromorphic photonic networks using silicon photonic weight banks," *Sci. Rep.*, vol. 7, Aug. 2017, Art. no. 7430.

[13] S. Y. Xiang *et al.*, "Cascadable neuron-like spiking dynamics in coupled VCSELs subject to orthogonally polarized optical pulse injection," *IEEE J. Sel. Topics Quantum Electron.*, vol. 23, no. 6, Nov./Dec. 2017, Art. no. 1700207.

[14] T. Deng, J. Robertson, and A. Hurtado, "Controlled propagation of spiking dynamics in vertical-cavity surface-emitting lasers: Towards neuromorphic photonic networks," *IEEE J. Sel. Topics Quantum Electron.*, vol. 23, no. 6, Nov./Dec. 2017, Art. no. 1800408.

[15] Y. Zhang, S. Xiang, J. Gong, X. Guo, A. Wen, and Y. Hao, "Spike encoding and storage properties in mutually coupled vertical-cavity surface-emitting lasers subject to optical pulse injection," *Appl. Opt.*, vol. 57, no. 7, pp. 1731–1737, Mar. 2018.

[16] S. Xiang, Y. Zhang, X. Guo, A. Wen, and Y. Hao, "Photonic generation of neuron-like dynamics using VCSELs subject to double polarized optical injection," *J. Lightw. Technol.*, vol. 36, no. 19, pp. 4227–4234, Oct. 1, 2018.

[17] M. P. Fok, Y. Tian, D. Rosenbluth, and P. R. Prucnal, "Pulse lead/lag timing detection for adaptive feedback and control based on optical spike-timing-dependent plasticity," *Opt. Lett.*, vol. 38, no. 4, pp. 419–421, Feb. 2013.

[18] R. Toole and M. P. Fok, "Photonic implementation of a neuronal algorithm applicable towards angle of arrival detection and localization," *Opt. Express*, vol. 23, no. 12, pp. 16133–16141, Jun. 2015.

[19] Q. Ren, Y. Zhang, R. Wang, and J. Zhao, "Optical spike-timing-dependent plasticity with weight-dependent learning window and reward modulation," *Opt. Express*, vol. 23, no. 19, pp. 25247–25258, Sep. 2015.

[20] R. Toole *et al.*, "Photonic implementation of spike-timing-dependent plasticity and learning algorithms of biological neural systems," *J. Lightw. Technol.*, vol. 34, no. 2, pp. 470–476, Jan. 15, 2016.

[21] Q. Li, Z. Wang, Y. Le, C. Sun, X. Song, and C. Wu, "Optical implementation of neural learning algorithms based on cross-gain modulation in a semiconductor optical amplifier," *Proc. SPIE*, vol. 10019, pp. 100190E-1–100190E-6, Oct. 2016.
AQ:1 = Please confirm the volume no. for ref. [21].

[22] S. Kuai and A. Meldrum, "Rapid color-switching micro-LEDs from silicon MIS diodes," *Phys. E, Low-Dimensional Syst. Nanostruct.*, vol. 41, no. 6, pp. 916–919, May 2009.

[23] K. Xu, "Integrated silicon directly modulated light source using p-well in standard CMOS technology," *IEEE Sensors J.*, vol. 16, no. 16, pp. 6184–6191, Aug. 2016.

[24] N. Li, H. Susanto, B. R. Cemlyn, I. D. Henning, and M. J. Adams, "Stability and bifurcation analysis of spin-polarized vertical-cavity surface-emitting lasers," *Phys. Rev. A, Gen. Phys.*, vol. 96, no. 1, p. 013840, Jul. 2017.

[25] K. Xu, "Monolithically integrated Si gate-controlled light-emitting device: Science and properties," *J. Opt.*, vol. 20, no. 2, p. 024014, Jan. 2018.

[26] X. Yan, X. Zou, W. Pan, L. Yan, and J. Azaña, "Fully digital programmable optical frequency comb generation and application," *Opt. Lett.*, vol. 43, no. 2, pp. 283–286, Jan. 2018.

[27] K. Xu *et al.*, "Light emission from a poly-silicon device with carrier injection engineering," *Mater. Sci. Eng. B*, vol. 231, pp. 28–31, May 2018.

[28] K. Iga, "Forty years of vertical-cavity surface-emitting laser: Invention and innovation," *Jpn. J. Appl. Phys.*, vol. 57, no. 8S2, p. 08PA01, Jul. 2018.

[29] X. Zou *et al.*, "Microwave photonics for featured applications in high-speed railways: Communications, detection, and sensing," *J. Lightw. Technol.*, vol. 36, no. 19, pp. 4337–4346, Oct. 1, 2018.

[30] A. Hurtado, A. Gonzalez-Marcos, I. D. Henning, and M. J. Adams, "Optical bistability and nonlinear gain in 1.55 μm VCSOA," *Electron. Lett.*, vol. 42, no. 8, pp. 483–484, Apr. 2006.

[31] A. Hurtado, I. D. Henning, and M. J. Adams, "Effects of parallel and orthogonal polarization on nonlinear optical characteristics of a 1550 nm VCSOA," *Opt. Express*, vol. 15, no. 14, pp. 9084–9089, Jul. 2007.

[32] A. Hurtado and M. J. Adams, "Two-wavelength switching with 1550 nm semiconductor laser amplifiers," *J. Opt. Netw.*, vol. 6, no. 5, pp. 434–441, May 2007.
[33] C. Tombling, T. Saitoh, and T. Mukai, "Performance predictions for vertical-cavity semiconductor laser amplifiers," *IEEE J. Quantum Electron.*, vol. 30, no. 11, pp. 2491–2499, Nov. 1994.
[34] J. Piprek, S. Björlin, and J. E. Bowers, "Design and analysis of vertical-cavity semiconductor optical amplifiers," *IEEE J. Quantum Electron.*, vol. 37, no. 1, pp. 127–134, Jan. 2001.
[35] P. Royo, R. Koda, and L. A. Coldren, "Vertical cavity semiconductor optical amplifiers: Comparison of Fabry-Pérot and rate equation approaches," *IEEE J. Quantum Electron.*, vol. 38, no. 3, pp. 279–284, Mar. 2002.
[36] M. D. Sánchez, P. Wen, M. Gross, and S. C. Esener, "Rate Equations for modeling dispersive nonlinearity in Fabry-Pérot semiconductor optical amplifiers," *Opt. Express*, vol. 11, no. 21, pp. 2689–2696, Oct. 2003.
[37] P. Wen, M. D. Sánchez, M. Gross, and S. C. Esener, "Optical bistability in vertical-cavity semiconductor optical amplifiers," *App. Opt.*, vol. 45, no. 25, pp. 6349–6357, Sep. 2006.
[38] V. Gauss, A. Hurtado, D. Jorgesen, M. J. Adams, and S. Esener, "Static and dynamic analysis of an all-optical inverter based on a vertical cavity semiconductor optical amplifier (VCSOA)," *Opt. Commun.*, vol. 284, no. 9, pp. 2345–2350, May 2011.
[39] M. J. Adams, J. V. Collins, and I. D. Henning, "Analysis of semiconductor laser optical amplifiers," *IEE Proc. J.-Optoelectronics*, vol. 132, no. 1, pp. 58–63, Feb. 1985.

Shuiying Xiang was born in Ji'an, China, in 1986. She received the Ph.D. degree from Southwest Jiaotong University, Chengdu, China, in 2013.

She is currently an Associate Professor with the State Key Laboratory of Integrated Service Networks, Xidian University, Xi'an, China. She has authored or co-authored more than 60 research papers. Her research interests include vertical cavity surface-emitting lasers, neuromorphic photonic systems, brain-inspired information processing, chaotic optical communication, and semiconductor lasers dynamics.

Junkai Gong was born in Yulin, China, in 1993. He is currently pursuing the M.S. degree from Xidian University, Xi'an, China. His researching interest is the photonic spiking neural network and optical STDP.

Yahui Zhang was born in Zhangjiakou, China, in 1993. She is currently pursuing the Ph.D. degree from Xidian University, Xi'an, China. Her researching interest is the vertical cavity surface-emitting lasers and neuromorphic photonic systems.

Xingxing Guo was born in Ji'an, China, in 1993. She is currently pursuing the M.S. degree from Xidian University, Xi'an, China. Her researching interest is the dynamics and applications of semiconductor lasers.

Yanan Han was born in Guyuan, China, in 1996. She is currently pursuing the M.S. degree from Xidian University, Xi'an, China. Her researching interest is the dynamics and applications of semiconductor lasers.

Aijun Wen was born in Xi'an, China, in 1968. He received the Ph.D. degree from Xidian University, Xi'an, in 1998.

He is currently a Professor with the State Key Laboratory of Integrated Service Networks, Xidian University, Xi'an. His current research interests include microwave photonics and optical communication.

Yue Hao was born in Chongqing, China, in 1958. He received the Ph.D. degree from Xi'an Jiaotong University, Xi'an, China, in 1991.

He is currently a Professor with the State Key Discipline Laboratory of Wide Bandgap Semiconductor Technology, School of Microelectronics, Xidian University, Xi'an. His research interests include wide forbidden band semiconductor materials and devices, semiconductor device reliability physics and failure mechanism, and terahertz semiconductor materials and device.